RSC Advances

ROYAL SOCIETY OF CHEMISTRY

www.rsc.org/advances

Synthesis of Single-Crystalline NdB_6 Submicroawls via a Simple Flux-Controlled Self-Catalyzed Method

Wei Han[a], Hao Zhang[b], Jian Chen[b,*],Yanming Zhao[a,*], Qinghua Fan[a], Qidong Li[a]

[a]State Key Laboratory of Luminescent Materials and Devices, South China University of Technology, Guangzhou, 510641, PR China

[b]Instrumental Analysis and Research Centre, Sun Yat-Sen University, Guangzhou, 510275, PR China

*Corresponding author. E-mail: puscj@mail.sysu.edu.cn; zhaoym@scut.edu.cn

Abstract

Neodymium hexaboride (NdB_6) submicroawls have been fabricated via a simple flux-controlled self-catalyzed method using neodymium (Nd) powders and boron trichloride (BCl_3) as starting materials at 1000 ºC. Scanning electron microscopy (SEM) reveals that the submicroawls are tapered, with a length of 2-5μm and a diameter ranging from approximately 0.1-0.3μm at the root and 5-50nm at the tips. Transmission electron microscopy (TEM) shows that the submicroawls are single crystalline with the preferred growth direction along [001]. For a systematic research, we have discussed the morphological change of NdB_6 submicron structures by varying reaction temperatures, catalysts and duration. Moreover, a multistage growth model of the NdB_6 submicroawls is proposed.

Key words: Neodymium hexaboride; Submicroawls; Self-catalyzed

I. Introduction

One-dimensional (1D) rare-earth hexaboride (RB_6) nanostructures have been considered as the most promising candidates with excellent properties for field emitters, not only because of their outstanding mechanical properties, high melting points, low volatility at high temperature, high brightness and high chemical stabilities but also due to their high aspect ratio and relatively low work function [1-3]. It is known that materials with anisotropic structures and sharp tips or edges can greatly increase the emission current. Anisotropic nanostructures are better field emitters [4-5] where the emission current is strongly dependent upon the work function of the emitter surface, the radius of curvature of the emitter apex and the emission area [6-7]. The Fowler-Nordheim (F-N) theory [4] predicts that electron emitters made of materials with a low work function, higher aspect ratio and higher curvature of the tips, could greatly enhance the field emission (FE) current with a lower applied turn-on voltage.

As one of the rare earth hexaboride family members, neodymium hexaboride (NdB_6) has been reported to have a lower work function (1.6eV) [8] than many previously reported cathode materials, including RB_6 (LaB_6~2.7eV [9]; CeB_6~2.5eV [10]), ZnO (5.3eV) [11] and widely used tungsten (4.6eV) [12]. If single-crystalline NdB_6 nanostructures with high aspect ratio morphology, such as nanowires or nanotubes, can be fabricated, it may be an ideal candidate for the investigation and development of advanced field emission theory, and efficient cathodes for vacuum electronic devices. Recently, Wang developed a palladium-nanoparticle-catalyzed chemical vapor deposition (CVD) method to synthesize NdB_6 nanoobelisks and nanowires [13], but the boron precursor ($B_{10}H_{14}$) was toxic and the Pd-Nd-B alloy drops on the tips would limit the electron emission and reduce the current density [14]. Very recently, Xu et al. reported the synthesis of NdB_6 nanowires and nanoneedles via a catalyst-free CVD approach [15]. However, the boron source they used was highly poisonous and combustible diborane (B_2H_6), which required more stringent safety methods for storage and waste disposal. Therefore, a more effective and safer method to

synthesize NdB_6 nanostructures should be developed.

In this paper, we report the synthesis of the NdB_6 submicroawls via a simple flux-controlled self-catalyzed method [16-18]. Scanning electron microscopy (SEM) reveals that the submicroawls are tapered, with a length of 3-5μm and a diameter ranging from approximately 0.1-0.3μm at the roots and 5-50nm at the tips. Transmission electron microscopy (TEM) shows that the submicroawls are single crystalline with the preferred growth direction along [001]. Moreover, we have discussed the morphological change of NdB_6 submicron structures at different reaction temperatures, catalysts and duration time. In addition, a multistage growth model of the NdB_6 submicroawls is proposed.

II. Experimental Section

The NdB_6 awl-like submicrostructures were prepared by a self-catalyzed scheme [16] via a simple flux-controlled method with neodymium and boron trichloride as the source materials. The synthesis was based on the following chemical reaction: $Nd(s) + 6BCl_3(g) + 9H_2(g) = NdB_6(s) + 18HCl(g)$. The synthesis was performed in a horizontal high-temperature tube furnace (Shenjia Kiln, Luoyang, China). The real temperature in the flat-temperature zone was measured by a thermocouple which was mounted at the center of the tube. The silicon ((100) plane, Empak, USA) substrates ($8\times8mm^2$) were used for the experiments. They were ultrasonically cleaned using distilled water and ethanol. The Si substrates were then loaded inside a quartz boat. Precursor Nd metal powders (weight 0.5mg, purity 99.9%, particle size less than 96μm, Institute of Rare Earths, Baotou, China) were well deposited on the Si substrates. The quartz boat was then quickly placed into the flat-temperature zone of the horizontal tube furnace, and the furnace tube was purged with high-purity gas mixture (50%H_2+50%Ar, 99.99%, Ruimin Gas, Guangzhou, China) for 2h before heating to eliminate any oxygen in the furnace. The tube temperature was heated to 1000~1100ºC at 10 ºC/min with a 50 sccm (standard cubic centimeters per minute) continuous flow of gas mixture (50%H_2+50%Ar) and kept at this temperature for 50

min. When the tube reached the desired temperature, a steady BCl_3 (99.99%, Summit Specialty Gases, Tianjin, China) flow of 20 sccm was introduced to the tube for 30~40 min and then the BCl_3 flow was switched off in order to reduce the flux of B (active boron). After the reaction, the tube was cooled down to room temperature in 5 h under the 50%H_2+50%Ar mixed gas atmosphere. All the experiments were carried out at 1 atm. Then the products were washed with diluted hydrochloric acid and distilled water for several times to remove the potential impurities (Nd_2O_3, H_3BO_3). After drying at 60 ºC for 1 h, the final gray products were obtained. Four representative samples with different morphologies (submicroawl, submicrotube, submicrowire and submicrorod) were fabricated by varying some experimental parameters, and the detailed growth conditions are presented in the following context.

The products were characterized and analyzed by X-ray diffraction (XRD, TD-3500), field emission scanning electron microscopy (FE-SEM, Navo NanoSEM430), high resolution transmission electron microscopy (HRTEM, JEM-2010HR) installed with energy dispersive X-Ray spectroscopy (EDX, Oxford), and selected area electron diffraction (SAED, JEM-2010HR).

III. Results

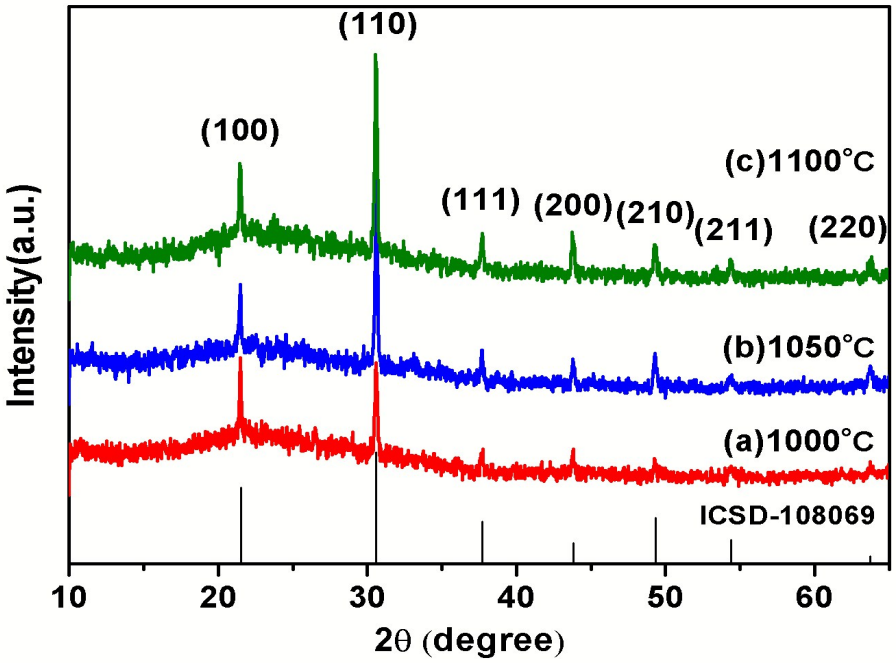

Figure 1. XRD patterns of the as-synthesized NdB_6 submicron structures at various temperatures: (a) 1000 ºC; (b) 1050 ºC; (c) 1100 ºC.

The phase identification of the product was carried out using X-ray powder diffraction. Shown in Figure 1 are the X-ray diffraction (XRD) patterns of the obtained NdB_6 submicron structures at various temperatures with catalyst-free: (a) 1000 ºC; (b) 1050 ºC; (c) 1100 ºC and the standard NdB_6 powder diffraction pattern from the Inorganic Crystal Structure Database (ICSD, NO. 108069) (bottom curve). No characteristic peaks of impurities are detected, indicating the purity of the products. All the diffraction peaks can be indexed by using Dicvol program and assigned to the lattice planes of (100), (110), (111), (200), (210), (211), (220) for the corresponding "d" spacing. The calculated lattice parameters of cubic NdB_6 obtained in 1000 ºC, 1050 ºC and 1100 ºC are 0.412(2)nm, 0.412(6)nm and 0.412(8)nm, respectively. The results agree with the standard NdB_6 powder diffraction lattice parameters of a=0.412(8)nm and a space group of $Pm\bar{3}m$.

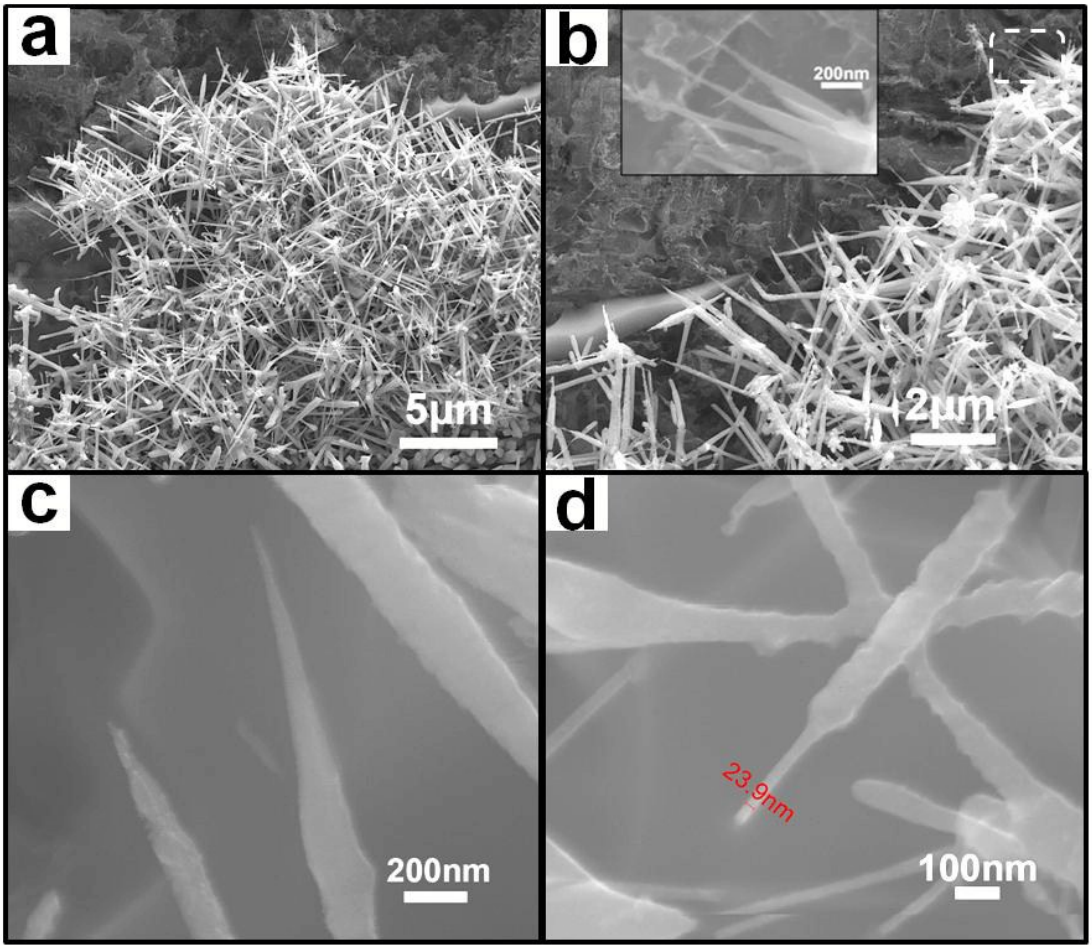

Figure 2. SEM images of the NdB_6 submicroawls obtained at 1000 ºC for 50min (BCl_3 duration 40min). (a, b) Submicroawls with tapering morphology. The inset shows an enlarged view of the submicroawls. (c) A typical submicroawl structure with a sharp tip. (d) A screwdriver-like submicroawl morphlolgy.

Figure 2 shows the typical SEM images of the NdB_6 submicroawls obtained on the Si substrates at 1000 ºC with a reaction time of 50min where the duration time of a flow of BCl_3 (20 sccm) is 40min. The low-magnification image of Figure 2a reveals that the final product is composed of submicroawls in a uniform morphology. The submicroawls are straight and about 2-5μm in length. Figure 2b shows most of the submicroawls are tapered. Figure 2b inset is a higher- magnification image, showing that the awl-handles have an average diameter of 0.15μm, and the awl tips have a diameter in a range of 5-50nm. Due to the handle-to-tip diameter ratios of 3 to 30, we call them submicroawls. As demonstrated in Figure 2c and 2d, the products can be classified into two types of awl-like morphology according to their tips. The tip of the

submicroawl in Figure 2c is extremely sharp and tapered, while the tip of the submicroawl in Figure 2d is very straight and the entire submicroawl is just like a screwdriver. Obviously, these submicroawls possessing extremely sharp tips are very important and beneficial for field-induced electron emission. It is noticeable that no catalytic particles can be observed at the tips of the submicroawls. Due to the absence of silicon-containing nanoparticles or other metal catalysts in our products, we conclude that the growth of submicroawls occurred directly on the Nd metal which acted as neodymium source and catalyst contemporaneously. In other words, the growth process of the submicroawls is attributed to the self-catalyzed mechanism.

The detailed information regarding the crystallinity, morphology, chemical composition, and growth direction of the NdB_6 submicroawls were further characterized by transmission electron microscopy (TEM) [19]. Figure 3 illustrates typical zoom-in TEM images of two single NdB_6 submicroawls. Figure 3a shows that the submicroawl is tapered from bottom to top and it has an ultra-sharp tip with a diameter of about 5nm. Moreover, no obvious particles can be observed from the tip of the submicroawl, which implies that no extra catalyst is involved during the synthesis process. Figure 3b reveals that this submicroawl is grown in the preferred [001] crystallographic direction of the cubic NdB_6 with lattice parameter of a=0.412(3)nm. The selected area electron diffraction (SAED) image (Figure 3c) along the $[\bar{1}10]$ crystal zone axis shows regular diffraction spots such as (110), (001) and (111) planes. The diffraction pattern appears identical as we moved the SAED aperture along the entire submicroawl, suggesting that the NdB_6 submicroawl is single crystalline. The EDX (Figure 3d) indicates that the submicroawl consists of Nd and B compositions with the molar ratio ~1:6 and no other impurity can be found. In order to explore the growth mechanism of the NdB_6 submicroawls, the detailed atomic structure around the tip of another submicroawl (see the inset of Figure 3 e) has been analyzed. Figure 3e shows that the tip of the NdB_6 submicroawl is ladder-shaped, and it is terminated by several different lattice planes that are marked with letters F to H on the image. The corresponding HRTEM images are showed in Figures 3f-h.

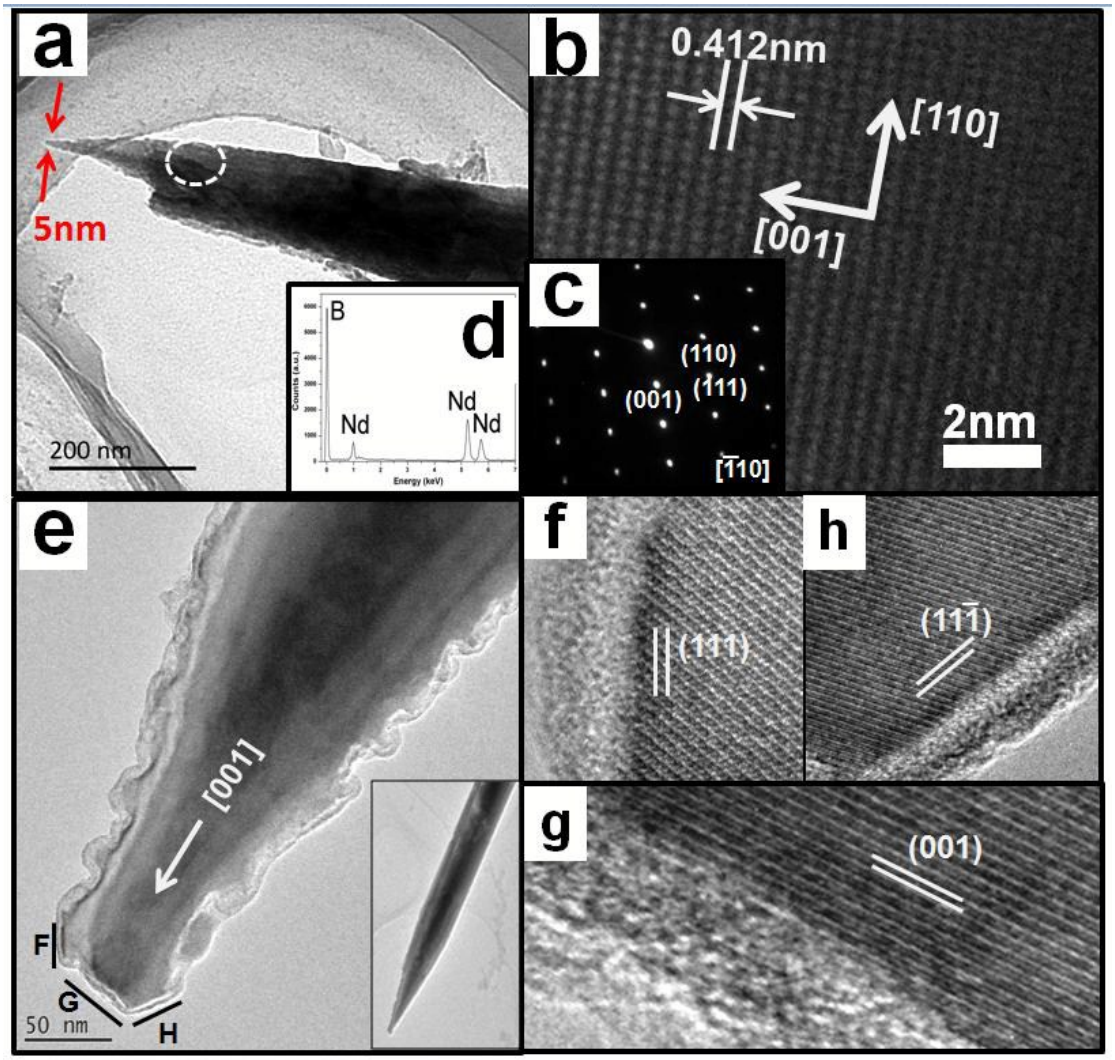

Figure 3. (a) TEM image of a single NdB_6 submicroawl; (b) HRTEM image of submicroawl bulk; (c) The corresponding SAED pattern; (d) The EDX spectrum taken from the submicroawl; (e) The NdB_6 submicroawl tip with terminating facets marked with letters F-H; (f-h) Lattice images of facets F-H as indicated in (e).

Figure 3f shows the lateral lattice of the tip marked with letter F in Figure 3e, which is terminated with the (111) lattice plane. Figure 3g shows a (001) facet, which is perpendicular to the submicroawl axis [001]. The [001] growth of these NdB_6 submicroawls is attributed to the fact that the {001} lattice planes of NdB_6 have the highest atomic density, and therefore, it would minimize the total energy for the crystal to grow in this lattice direction [2]. Figure 3h shows (11-1) facet corresponding to the area marked with H in Figure 3e. The above results indicate that the {001}, {111} and {11-1} type planes with low indices are the dominant terminating lattice planes which agree with the lowest energy principle in crystal growth. Moreover, it is

reasonable that the growth rate of lateral lattices (111) and (11-1) is slowing down during the last stage, because the tip is grown at the last stage when the flux concentration of BCl_3 is decreasing. This result will give rise to the reduction in the ratio of lateral vs. vertical growth, leading to the tapered structures.

IV. Discussion

To explore the growth mechanism of as-synthesized NdB_6 submicroawls, a series of systematic experiments were carried out to study the effects of reaction temperatures, catalytic materials and reaction duration. A "self-catalyzed" growth mechanism was proposed based on the experimental results.

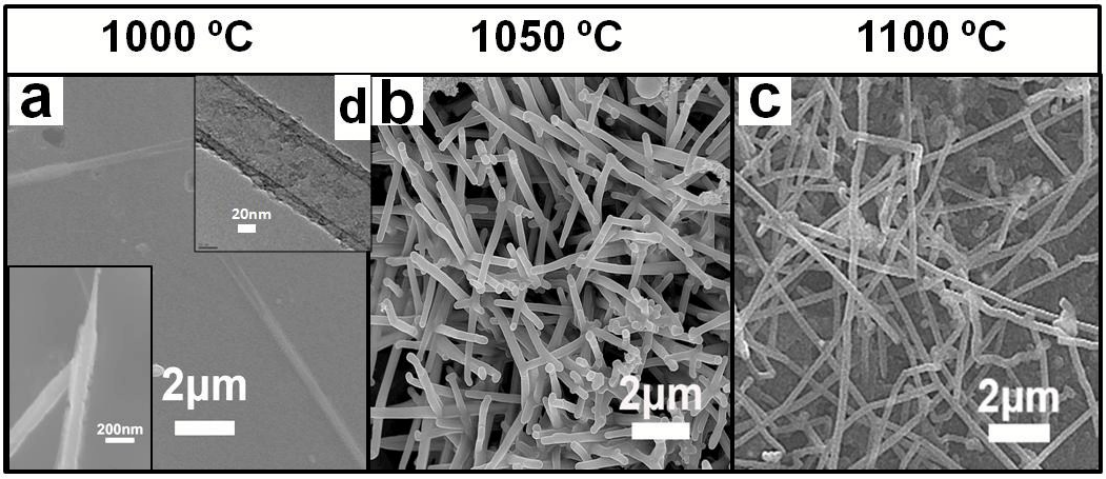

Figure 4. SEM images of NdB_6 1D submicron structures at various temperatures: (a) submicroawls and submicrotubes at 1000 ºC; (b) submicrorods at 1050 ºC; (c) submicrowires at 1100 ºC. (d) TEM image of the NdB_6 submicrotube.

1. Effect of Reaction Temperatures. The morphological structures of NdB_6 Submicron materials were found to be strongly influenced by the reaction temperatures to yield different 1D submicron structures — submicroawls, submicrotubes, submicrorods and submicrowires. With other parameters (i.e., reaction duration, flow rate and flow duration time, heating and cooling rate, catalyst-free, etc.) unchanged, the reaction temperatures were varied from 1000 ºC to 1100 ºC. XRD

patterns of the as-synthesized NdB_6 submicron structures at various temperatures are shown in Figure 1. Typically, at a low reaction temperature (1000 ºC), straight tapered submicroawls with length ranging from about 2-5μm are obtained (Figure 2, Figure 3 and Figure 4a inset). Besides, at this lower temperature (compared to the melting point 1024 ºC of metal neodymium) the NdB_6 submicrotubes with very small amount are also found on the substrate but in the different locations (Figure 4a). As it can be seen from Figure 4a, there are two NdB_6 submicrotubes which have diameters of 0.2-0.3μm and lengths of 10-20μm. In order to clearly recognize and confirm the tubular structure, the TEM image has been presented in Figure 4d where a hollow interior channel structure comes into view. As to the formation of tubular structures under a self-catalyzed mechanism, the related reports are few. A broad accepted growth model is proposed by Erick et al. who considered that the formation of hollow nanotubes can be ascribed to the diffusion limit in the droplet at high temperature, which results in the ring-shaped nucleation and induced the growth of nanotubes [20]. In this work, the growth mechanism of NdB_6 tubes is similar to the formation model of PrB_6 nanotubes [21].

At a reaction temperature of 1050 ºC, the NdB_6 submicron structures undergo a morphology transition from submicroawls/tubes to rods without tapered tips (Figure 4b). SEM images show that the average diameters and lengths of these rods are 0.15-0.3μm and 2-8μm. At the highest temperature (1100 ºC), NdB_6 submicrowires are grown instead (Figure 4c). The average length of ~20μm of the submicrowires is larger than that of the submicroawls grown at 1000 ºC and the submicrorods grown at 1050 ºC. These results are principally attributed to the enhancement of growth rates with the increasing temperature. Note that the submicroawls and submicrotubes can be only fabricated at 1000 ºC, so we infer that the reaction temperature may be the key factor for the growth of the two morphologies.

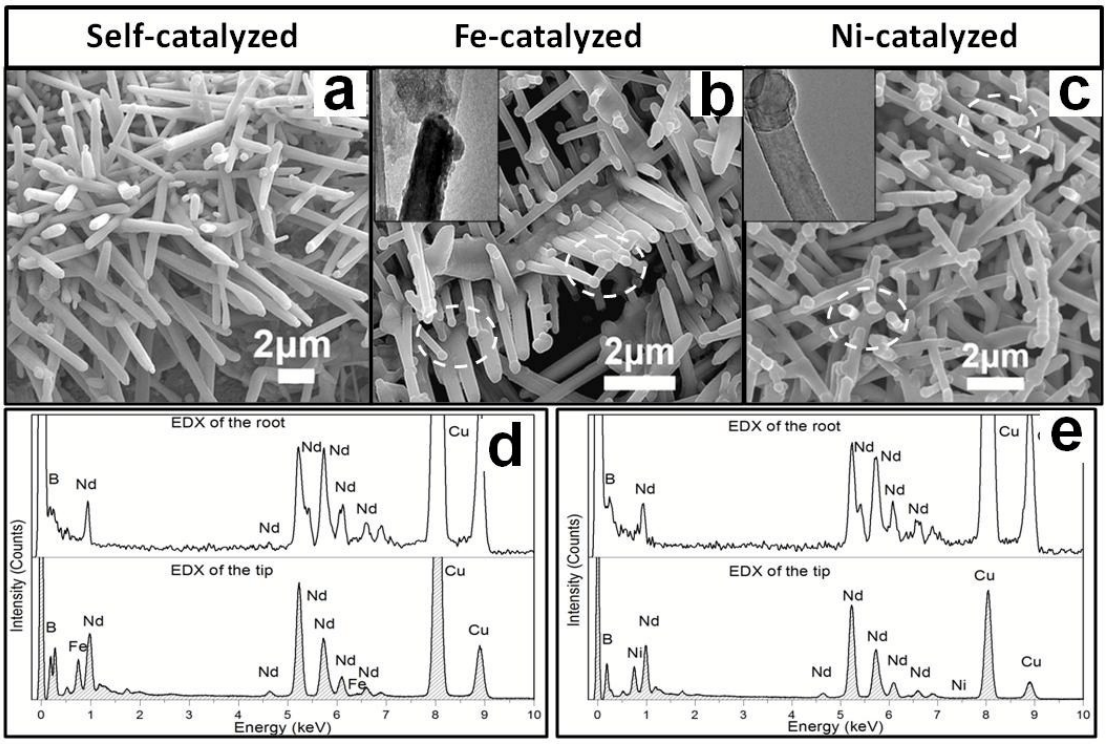

Figure 5. SEM images of NdB_6 submicrorods synthesized at 1050℃: (a) by self-catalyzed growth; (b) by Fe-catalyzed growth; (c) by Ni-catalyzed growth. (d) EDX spectrums of the tip and the root of the submicrorod shown in the (b) inset; (e) EDX spectrums of the tip and the root of the submicrorod shown in the (c) inset.

2. Effect of Catalytic Materials. To probe the effect of catalysts on NdB_6 products, we compared self-catalyzed growth (SCG) and metal-catalyzed growth (MCG) (M=Fe, Ni) at 1050℃. Here, the metal Fe/Ni was obtained from the high temperature reduction of $Fe(NO_3)_3/Ni(NO3)_2$ by H_2. The $Fe(NO_3)_3/Ni(NO3)_2$ film was coated on the Si substrates by a drop-casting method. 1D submicron structures can be identified from the substrates after both SCG and MCG. However, the morphologies of samples through these two methods are different. Typically, in a SCG method, long submicrorods with length ranging from about 2~8μm are obtained (Figure 5a & Fig. 4b). The diameter of these rods is about 150nm to 300nm. While using MCG method, we can obtain short straight rods with branches (Figure 5b & 5c). The diameter of these rods is about 50nm to 200nm. The average length of ~3μm of the rods in the sample is much shorter than the rods grown by the SCG method. Moreover, a small globule is present at the tip of the rod by the MCG method (circled in Figure 5b & 5c), while no globule can be observed at the tip of the rod by the SCG method (Figure 5a).

In order to confirm the existing of catalysts at the tips of those submicron structures, the TEM images are presented in the insets of Figure 5b &5c, where the small globules can be visible. Furthermore, the EDX was used to show the compositions at the tips of the as-synthesized submicrostructures. Figure 5d &5e and Figure 3d show the compositions of the as-synthesized submicrostructures with and without using catalysts during synthesis process. In Figure 5d & 5e, the signals of Fe and Ni are present in the EDX of the tips, and this result shows the catalytic materials are included in the tips. These results are maybe owing to the different growth mechanisms of these two methods. Hence, we hypothesize that the MCG method is dominated by a nontraditional VLS (vapor-liquid-solid) growth mechanism. Although detailed information on the ternary phase diagram of Nd-B-M is not available, small miscible Nd-B-M liquid alloy droplets may be formed and act as nucleation sites. The continuous supply of boron causes the liquid Nd-B-M droplets to become supersaturation, resulting in the precipitation of NdB_6 as rods by the VLS-like growth mechanism. Because of this process, the globules on the tips appears which is just similar to the Au-catalytic Si whisker growth and Sn-guided ZnO 1D nanostructure growth [22, 23]. However, there are no globules found in the SCG method owing to the different mechanism in the following discussion. In addition to Fe and Ni, other catalytic material such as platinum (Pt) was employed in experiments (not shown here). Fe was found to have the highest catalytic efficiency, followed by Ni and Pt. Furthermore, the compositions at the roots were also studied (Figure 5d & 5e) and compared to those at the tips. No signals of Fe and Ni observed at the root of the as-synthesized structures suggests that these structures are grown by the tip-based VLS mechanism.

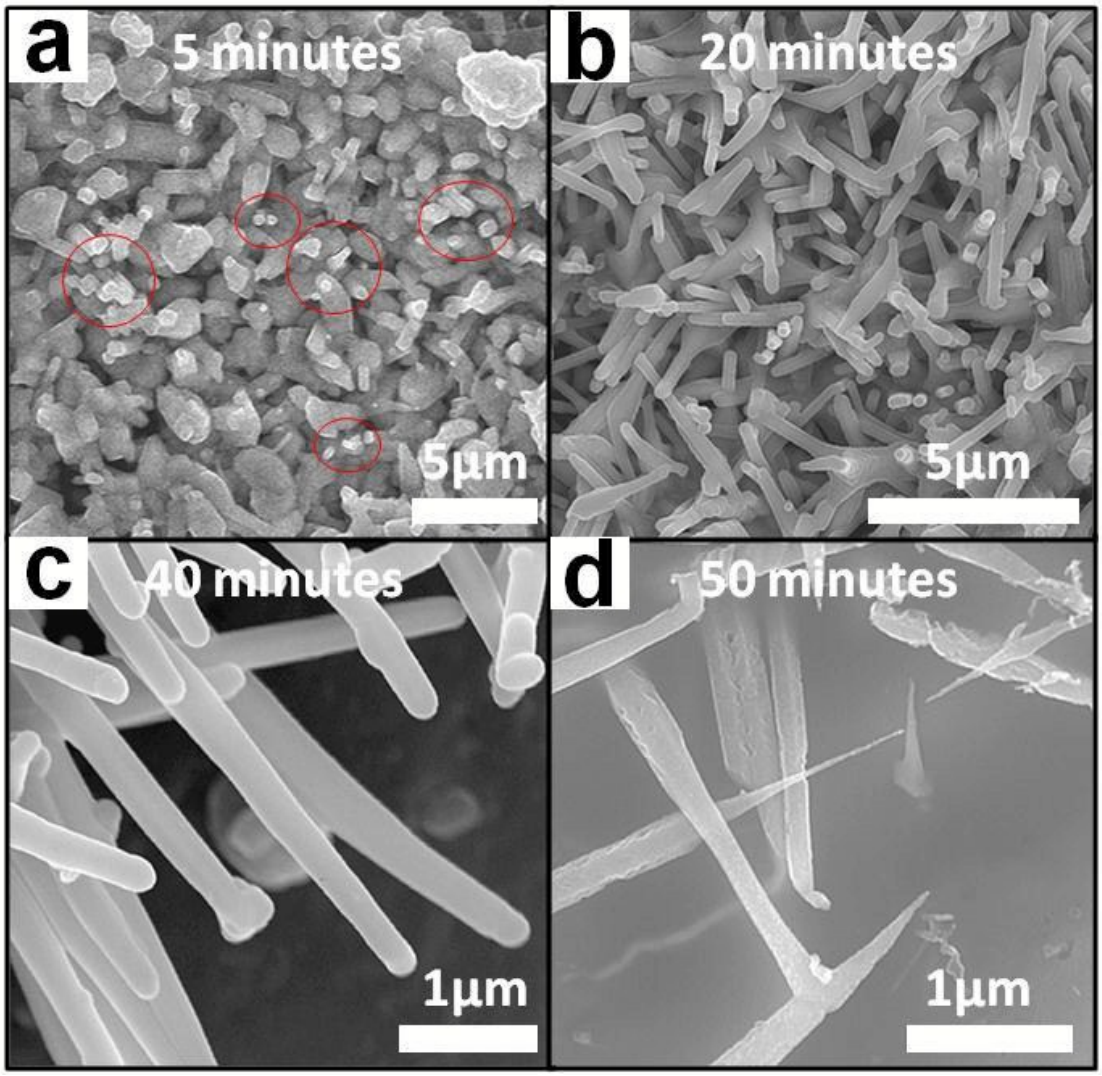

Figure 6. The time-dependent morphological evolution of NdB_6 submicroawls synthesized at 1000 ºC. SEM images of the samples prepared with duration: (a) 5 minutes; (b) 20 minutes; (c) 40 minutes; (d) 50 minutes (switching off BCl_3 at 40 minutes). The circles in (a) are the location of initial growth of submicron materials.

3. Effect of Reaction Duration. A time trial growth study was conducted for further insight into the catalyst-free growth of the submicroawls at 1000 ºC. Here, the reaction duration was adopted as 5min, 20min, 40min and 50 min and the corresponding duration time of a flow of BCl_3 (20 sccm) was 5min, 20min, 40min and 40 min, respectively. The time-dependent morphological evolution of NdB_6 submicroawls is shown in Figure 6. Initially, for submicron structures grown with a

shorter reaction time (5 min), a thin layer of cubic-shaped film of NdB_6 was deposited on the silicon substrate. Moreover, some short rods (marked by the circles in (a)) can be identified (Figure 6a). As discussed later in the text, it is believed that the film and short rods are the nucleation and initial growth of NdB_6 which plays an important role for further growth of NdB_6 1D submicron structures. For submicron structures grown with an intermediate reaction time (20 min), thicker and longer 1D submicron structures are obtained as shown in Figure 6b. In this period, the observed increase in the heights and widths of the materials suggests the growth process followed a continuous self-catalyzed vertical growth with lateral growth. During the 40 min growth period, the tips of the wires are not tapered (Figure 6c). However, the evolution of these wires into awl structures occurred between the 40-50 min reaction period after the BCl_3 gas was switched off (Figure 6d). As BCl_3 precursor flux was very important for the growth of 1D submicron structures, so it could be assumed that the BCl_3 flux was a key factor for the formation of submicroawls. Once the BCl_3 precursor was switched off, the local concentration at the growth zone decreased until the remaining BCl_3 flow was completely exhausted. This decrease in concentration gradient was expected to cause a decrease in the ratio of lateral vs. vertical growth, leading to the growth of tapered tops of the submicroawls. In short, time-dependent morphological evolution of NdB_6 1D submicron structures was revealed, and the results are beneficial for the further understanding of possible growth mechanism of the submicroawls.

4. Growth Mechanism.

SEM and TEM analysis show that the growth of the submicroawls may not be governed by the conventional VLS process proposed that the nanowires grew by the catalytic-assisted approach, in which a metal particle is located at the growth front of the wire and acts as the catalytic active site. Moreover, no catalytic particles are found on the tips of the submicroawls, and it is likely that the growth is dominated by a "self-catalyzed" mechanism [16-18, 21]. In this work, melting metal Nd plays the roles of both raw material and catalyst simultaneously in the process of synthesizing NdB_6

submicroawls. Four main steps involved in the growth for the submicroawls are outlined as following (Figure 7a-d).

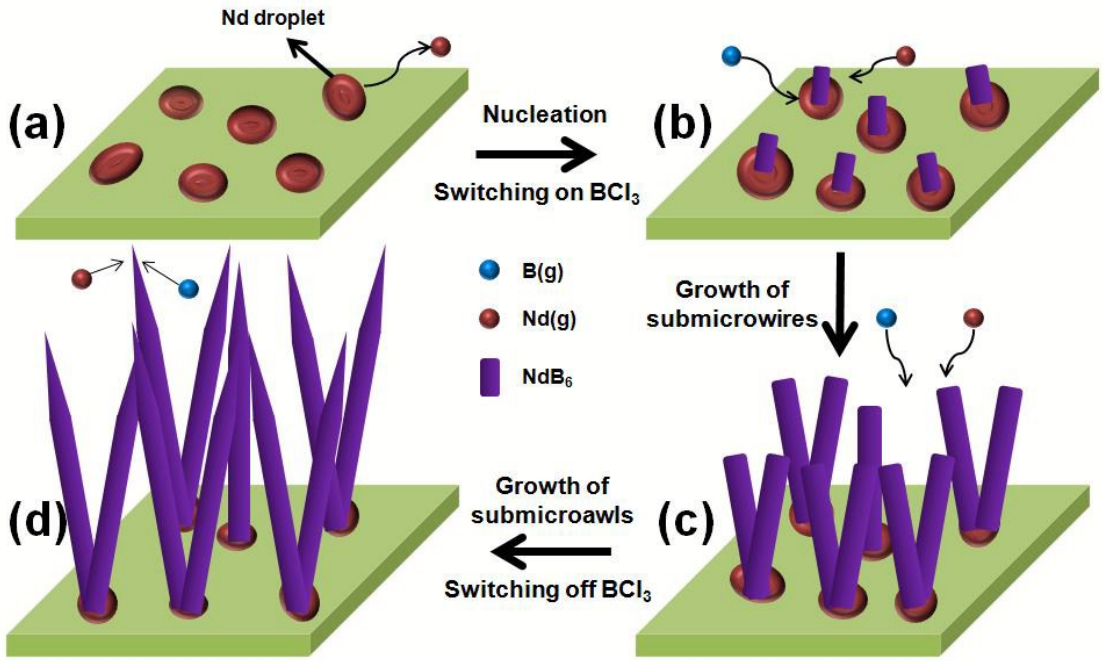

Figure 7. A schematic of a possible growth model for the NdB_6 submicroawls synthesized at 1000 ºC. (a) Formation of metal Nd liquid droplets Nd vapor; (b) Nucleation and initial growth of NdB_6 crystal; (c) Continuous growth of NdB_6 submicrowires; (d) Growth of NdB_6 submicroawls.

(1) Generation of Nd liquid phase and vapor phase.

At elevated temperature (approaching or higher than the Nd melting point of 1024 ºC), the solid Nd particles become liquid droplets as source materials at the original sites. Meanwhile, the vaporization of Nd powders also generates Nd vapor (Figure 7a). We note that, according to the literature, the vapor pressure of the Nd metal is low (~5.7 $\times 10^{-2}$ Pa) at the reaction temperature we used (~1000 ºC)[24]. Here, the low concentration of Nd vapor should exist which can take part in the growth of 1D submicron structures because NdB_6 wires can be also observed at the edge of the Si substrate as illustrated in Figure 8a where no Nd particles were coated. Therefore, Nd liquid droplets and Nd vapor can coexist as the source for the growth of NdB_6 1D submicron structures. In order to confirm the submicrowires are pure NdB_6, a set of controlled experiments have been done (see Figure S1). There are no other wires can

be found on the Si substrates, especially along the edges. Furthermore, the EDX shown in Figure 8b illustrates that NdB_6 submicrowires consist of Nd and B compositions, and no other element can be found.

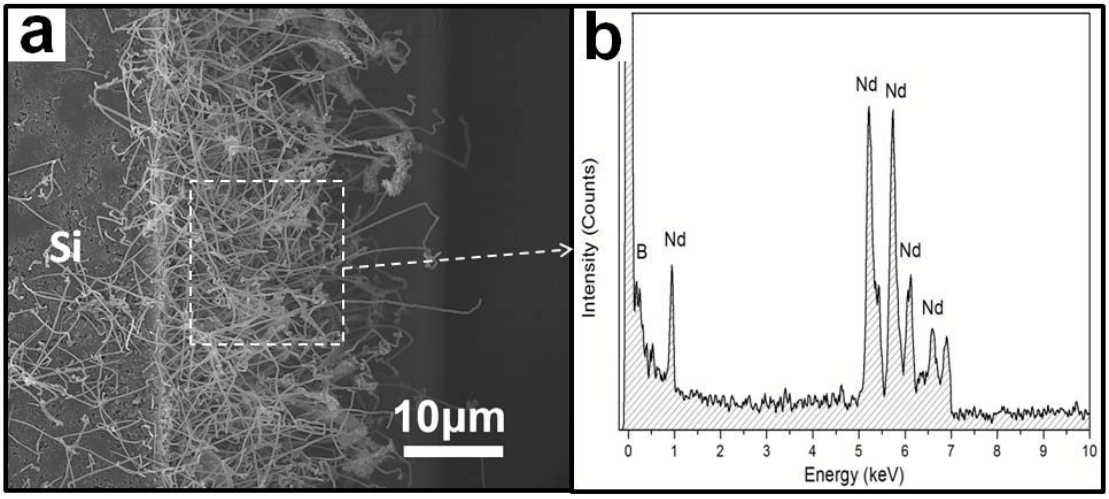

Figure 8. (a) SEM image of the NdB_6 submicrowires grown at the edge of the Si substrate; (b) EDX spectrum of the marked area in (a).

(2) Nucleation and initial growth of NdB_6 crystal.

When the furnace reached the setting temperature, BCl_3 was introduced into the reactor. The pyrolysis of BCl_3 can produce active B as a boron source ($2BCl_3 \rightarrow 2B+3Cl_2$). The active B will impinge upon the surfaces of Nd liquid droplets or Nd vapor and then be absorbed. Plenty of small miscible Nd-B liquid alloy droplets can be formed and act as nucleation sites. The liquid droplet is preferred site for absorption from the B, which cause the liquid to become supersaturated with NdB_6. With the sustained absorption of B, the initial crystal grows by precipitation of NdB_6 from the droplets. Meanwhile, a little Nd vapor and active B may react for the lateral growth (shown in Figure 7b).

(3) Continuous growth of NdB_6 submicrowire.

By a continuation of the above process the NdB_6 crystal grows from the nucleation sites and ascends atop the liquid droplets to form submicrowires, as shown in Figure7c. During this growth period, the increase in the length and width of the

submicrowires indicates the growth process followed a self-catalyzed vertical growth with lateral growth due to direct deposition. The submicrowires grow in length and width by this mechanism until the Nd or B is consumed.

(4) Growth of NdB_6 submicroawls.

In addition to the self-catalyzed (SC) mechanism [16], the vapor-solid (VS) growth [25] of NdB_6 submicrowires may exist in the reaction chamber. We suggest that the combination of SC and VS growth is responsible for the growth of tapered NdB_6 submicroawls (Figure 7d) at lower temperature (1000 ºC). The continuous growth of NdB_6 submicrowires along the longitudinal direction is achieved via the SC mechanism (as discussed above), whereas lateral growth is typically realized via the VS mechanism ($Nd+6B \rightarrow NdB_6$). In this scenario, the bottom portion of NdB_6 submicrowires formed at the earlier stages develops a larger diameter. However, when the BCl_3 is switching off in the later stage, the decrease in flux concentration of B will result in the reduction in the ratio of lateral vs. vertical growth, leading to the tapered structures observed by SEM/TEM. This multistage growth model is consistent with observations in growth experiments such as the multistage growth of LaB_6 nanoobelisks [26], ZnO nanotips [27] and ZnS nanoawls [28].

Conclusion

In summary, single-crystalline NdB_6 submicroawls were achieved via a simple flux-controlled self-catalyzed method. The tapered submicroawls had a length of 2-5μm and a diameter ranging from approximately 0.1-0.3μm at the roots and 5-50nm at the tips. Our results suggests that Nd liquid droplets and Nd vapor can coexist as the source for the growth of NdB_6 1D submicron structures although the reaction temperature of 1000 ºC is lower than the Nd melting point of 1024 ºC. Furthermore, a concentration gradient is necessary to create these awl-like structures where the combination of SC and VS growth is responsible for the growth of tapered NdB_6 submicroawls. Due to the poor conductivity of the Si substrates which resulted from the eroding by the BCl_3 gas to form the rough background [16], the work on the field

emission is difficult to conduct using the as-synthesized product. Further studies to reveal the effect of geometry for single submicroawls on their field-emission properties will be performed in the future. We expect that this work will arouse further interest and investigation of morphological control of submicrostructures and their properties.

Acknowledgments

This work was funded by NSFC Grant (No. 51172077, 51372089, 51373205) supported through NSFC Committee of China, the Foundation of (No. S2011020000521) supported through the Science and Technology Bureau of Guangdong Government and the Foundation of (No. 2014ZB0014) supported through the Fundamental Research Funds for the Central Universities.

References

(1) H. Zhang, Q. Zhang, J. Tang, and L. C. Qin, *J. Am. Chem. Soc.* 2005, **127**, 2862.

(2) H. Zhang, J. Tang, Q. Zhang, G. Zhao, G. Yang, J. Zhang, O. Zhou, and L. C. Qin, *Adv. Mater.* 2006, **18**, 87.

(3) H. Zhang, J. Tang, J. Yuan, J. Ma, N. Shinya, K. Nakajima, H. Murakami, T. Ohkubo, and L. C. Qin, *Nano Lett.* 2010, **10**, 3539.

(4) R.H. Fowler, L. Nordheim, *Proc. R. Soc. London* 1928, **119**, 173.

(5) W.A.D. Heer, A. Chatelain, D. Ugarte, *Science* 1995, **270**, 1179.

(6) L. Vila, P.I. Vincent, L.D. De Pra, G. Pirio, E. Minoux, L. Gangloff, S. Champagne, N. Sarazin, E. Ferain, R. Legras, L. Piraux, P. Legagneux, *Nano Lett.* 2004, **4**, 521.

(7) B. Varghese, T.C. Hoong, Z. Yanwu, M.V. Reddy, B.V.R. Chowdari, A.T.S. Wee,T.B.C. Vincent, C.T. Lim, C.H. Sow, *Adv. Funct. Mater.* 2007, **17**, 1932.

(8) P. H. Schmidt, L. D. Longinotti, D. C. Joy, S. D. Ferris, H. J. Leamy, Z.J. Fisk, *Vac. Sci. Technol.*1978, **15**, 1554.

(9) Yutani, A.; Kobayashi, A.; Kinbara, A. *Appl. Surf. Sci.*1993, **70**, 737.

(10) P. R. Davis, M. A. Gesley, G. A. Schwind, L. W. Swanson, J. Hutta, *J.Appl. Surf. Sci.*1989, **37**, 381.

(11) T. Minami, T. Miyata, T. Yamamoto, *Surf. Coat. Technol.*1998, **108**, 583.

(12) T. Kawakubo, Y. Shimoyama, H. Nakane, H. Adachi, *J. Vac.Sci. Technol. B,* 2008, **26**, 1395.

(13) G. Wang, J. R. Brewer, J. Y. Chan, D. R. Diercks, C. L. Cheung, *J. Phys. Chem. C* 2009, **113**, 10446.

(14) W. Zhu, G. P. Kochanski, S. Jin, *Science*, 1998, **282**, 1471

(15) J. Xu, G. Hou, T. Mori, H. Li, Y. Wang, Y. Chang, Y. Luo, B. Yu, Y. Ma, and T. Zhai, *Adv. Funct. Mater.* 2013, **23**, 5038.

(16) J. Xu, Y. Zhao, C. Zou, *Chem. Phys. Lett.* 2006, **423**, 138.

(17) Q. Ding, Y. Zhao, J. Xu, C. Zou, *Solid State Commun.* 2007, **141**, 53.

(18) Q. Fan, Q. Zhang, Y. Zhao, Q. Ding, *J. Rare Earths*, 2013, **31**, 145.

(19) Y. Ding, Z. L. Wang, *J. Phys. Chem. B*, 2004, **108**, 12280.

(20) E. P. A. M. Bakkers, M. A. Verheijen, *J. Am. Chem. Soc.* 2003,**125**, 3440.

(21) M. Chi, Y. Zhao, Q. Fan, W. Han, *Ceram. Int.* 2014, **40**, 8921.

(22) R. S. Wagner, W. C. Ellis, *Appl. Phys. Lett.*1964, **4**, 89.

(23) Y. Ding, P. X. Gao, Z. L. Wang, *J. Am. Chem. Soc.* 2004, **126**, 2066.

(24) C. E. Habermann, A. H. Daane, *J. Chem. Phys.*1964, **41**, 2818.

(25) Z. W. Pan, Z. R. Dai, Z. L. Wang, *Science* 2001, **291**, 1947.

(26) J. R. Brewer, N. Deo, Y. M. Wang, C. L. Cheung, *Chem. Mater.* 2007, 19, 6379.

(27) Z. Z. Yea, J. Y. Huang, W. Z. Xu, J. Zhou, Z. L. Wang, *Solid State Commun.* 2007, **141**, 464.

(28) T. Zhai, Z. Gu, H. Fu, Y. Ma, and J. Yao, *Cryst. Growth Des.* 2007, **7**, 1388.